

Cross Modal Global Local Representation Learning from Radiology Reports and X-Ray Chest Images

Nathan Hadjiyski^{*a}, Ali Vosoughi^{*b}, and Axel Wismüller^{b,c,d,e}

^aDepartment of Computer Science, University of Rochester, NY, USA

^bDepartment of Electrical and Computer Engineering, University of Rochester, NY, USA

^c Department of Imaging Sciences, University of Rochester, NY, USA

^dDepartment of Biomedical Engineering, University of Rochester, NY, USA

^eFaculty of Medicine and Institute of Clinical Radiology, Ludwig Maximilian University, Munich, Germany

*Authors with equal contributions.

ABSTRACT

Deep learning models can be applied successfully in real-work problems; however, training most of these models requires massive data. Recent methods use language and vision, but unfortunately, they rely on datasets that are not usually publicly available. Here we pave the way for further research in the multimodal language-vision domain for radiology. In this paper, we train a representation learning method that uses local and global representations of the language and vision through an attention mechanism and based on the publicly available Indiana University Radiology Report (IU-RR) dataset. Furthermore, we use the learned representations to diagnose five lung pathologies: atelectasis, cardiomegaly, edema, pleural effusion, and consolidation. Finally, we use both supervised and zero-shot classifications to extensively analyze the performance of the representation learning on the IU-RR dataset. Average Area Under the Curve (AUC) is used to evaluate the accuracy of the classifiers for classifying the five lung pathologies. The average AUC for classifying the five lung pathologies on the IU-RR test set ranged from 0.85 to 0.87 using the different training datasets, namely CheXpert and CheXphoto. These results compare favorably to other studies using UI-RR. Extensive experiments confirm consistent results for classifying lung pathologies using the multimodal global local representations of language and vision information.

Keywords: Deep learning, cross-modal learning, computer vision, natural language processing, zero-shot classification, chest X-ray, radiology reports

Further author information: (Send correspondence to Ali Vosoughi)
Ali Vosoughi: E-mail: mvosough@ece.rochester.edu

1. INTRODUCTION

Deep learning is prevalent thanks to its success in numerous real-life domains and surpassing classic techniques in performance, cost, and ease of applicability. However, despite the computational efficiency of deep learning models, it requires a massive amount of data, which is scarce and expensive, especially in radiology. Multimodal learning recently got considerable attention. Language is a widely available form of data in radiology besides images. Therefore, one can design deep learning models that use language and vision in different ways to improve the quality of medical image analysis, for instance, by using radiology reports to enhance the performance of downstream tasks through x-ray images.

This paper addresses multimodal representation learning from a combination of radiology reports and their corresponding medical images. We use x-ray images and radiology reports of a publicly available dataset and tailor it to learn a multimodal representation that encompasses local and global language and visual information. Although many recent methods consider language and vision in multimodal learning, one major problem in radiology’s vision and language models is the lack of sufficient datasets, which is well addressed in this paper. In many instances, the codes are publicly available without corresponding datasets, preventing further developments of the methods in the community [1].

In this paper, we learn multimodal representations of a publicly available dataset of IU-RR and modify and clean the dataset for learning global and sub-regional features of both images and radiology reports. We use a global-local representation framework that attends to both the image-sub-regions and word-piece language and global representations of vision and language modalities. Therefore, as a direct result of this research, radiology reports can be used to attend to related parts in the medical image and learn representations encompassing local and global details of x-ray images and corresponding descriptions. The architecture of the method is shown in Fig. 1.

The method here uses a small dataset of Indiana University Radiology Reports (IU-RR) [2]. Despite its smaller size than other datasets, such as Chexpert, we can train the model and perform downstream tasks such as classification in supervised and zero-shot approaches. Our method reaches an area under the curve performance (AUC) of 0.8618, which is slightly higher than the best existing datasets. Finally, we show that we can perform zero-shot classification using multimodal representations.

This work is embedded in our group’s endeavor to expedite artificial intelligence in biomedical imaging by means of advanced pattern recognition and machine learning methods for computational radiology and radiomics, *e.g.*, [3–86].

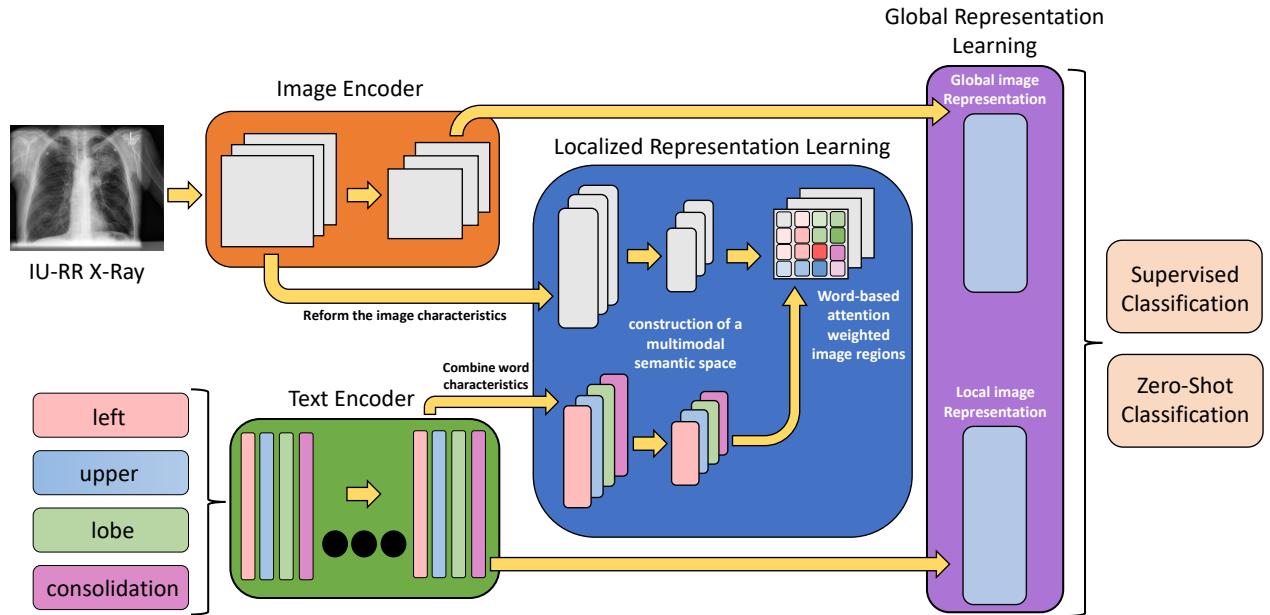


Figure 1: The architecture of multimodal deep representation learning is shown. The model encodes image and text features at global and local levels and then fuses this information to encompass both local and global details for later downstream tasks. The attention mechanism corresponds word-level features to image sub-regions by leveraging a similarity matrix between the local features of an image and its text. Global and local representations are learned through maximizing the posterior probability of the image given text and vice versa and using global and local contrastive learning.

2. ALGORITHM

2.1 Representation Learning Model

The GLoRIA model [1] was built on the premise that many anomalies observed in medical imaging tests only occupy a small portion of the image and only roughly match a handful of crucial sentences in medical reports. As a result, the model creates an attention-based framework for multimodal representation learning by contrasting image subregions to the words in the relevant report. This allows for the generation of context-aware local representations of pictures using attention weights that emphasize important visual sub-regions for a particular word. Seen in Fig. 1.

The model takes advantage of the final adaptive average pooling layer of the ResNet-50 model to help with the creation of Image Encoders. The GLoRIA text encoder was pretrained on the BioClinicalBERT model using medical texts from the MIMIC III dataset in order to produce clinically informed text embeddings. Additionally, word-piece tokenization was employed to lessen the embeddings of acronyms and some lexical problems in report drafting. The text encoder extracts feature specific to each word component. The global text feature is the

whole of all word-piece features. Through the use of global, semantic data that condenses the picture and report, and local, captures the semantics in the image and, features. Word-level embeddings are used for local text characteristics.

Supervised classification model: The model trains a linear classifier on top of the already-trained image encoder GLoRIA model to evaluate the data efficiency of the global picture representations.

Zero-shot classification: Zero-shot Classification analyzes the ability of our learned representations to be categorized without the addition of additional labels. The results of the Zero-shot Classification allow evaluation of how good the representations between reports and images within GLoRIA model are based on the achieved accuracy.

3. DATA

We used three different datasets in this study due to the lack of radiology reports for CheXpert and CheXphoto, and the smaller size of the IU-RR dataset with radiology reports. In the following, we briefly describe each of these datasets.

3.1 CheXpert

The CheXpert dataset [2] was used to train and evaluate the representation learning framework for the supervised classification tasks. The 224,316 chest radiographs from the 65,240 individuals in the CheXpert dataset are all linked with the associated radiology reports. A total of 14 medical observations is included on each radiograph’s label. This research used 191,229 frontal chest radiograph image-text pairings (original train: 191,027 and original valid: 202). Example of pictures seen in Fig. 2.

3.2 CheXphoto

CheXphoto dataset [87] is a noisy dataset comprised of a training set of natural images and synthetic transformations applied to 10,507 x-rays from 3,000 different patients that were randomly selected from the CheXpert training set. The validation and test sets are composed of 234 x-rays from 200 patients and 668 x-rays from 500 patients, respectively. The GLoRIA model only focuses on the frontal images, so for the CheXphoto, we focus on 28,718 images (original train: 28,112 and original valid: 606). Examples of x-ray images are shown in Fig. 2.

Both CheXpert and CheXphoto had labels provided for each of the diseases (positive = 1, negative = 0, unclear = -1). Although chest abnormalities are frequently suspected, a conclusive diagnosis cannot be obtained without further testing. However, at the time of this research, the CheXpert radiology reports were still under review for the protected health information review through the Health Insurance Portability and Accountability Act. The radiology reports were not available for both CheXpert and CheXphoto datasets.








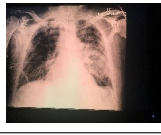







Dataset	Atelectasis	Cardiomegaly	Consolidation	Edema	Pleural Effusion
CheXpert [87]					
CheXphoto [88]					
IU-RR [2]					

Figure 2: Three datasets and their corresponding five types of lung diseases are shown in this image. The radiology reports of CheXpert [87] and CheXphoto [88] are not publicly available, while IU-RR [2] are labeled images and their corresponding radiology reports. Despite the smaller size of the IU-RR dataset, we could learn multimodal representations from the IU-RR dataset.

3.3 Chest X-Ray Collection from Indiana University

The open-access chest X-ray collection from Indiana University (IU-RR) [88] consists of 3,996 radiology reports from the Indiana Network for Patient Care and 8,121 associated images from the hospitals’ picture archiving systems. The GLORIA model only focuses on the frontal images so for the Indiana dataset, and we focus on 3,279 images with reports (original train: 2,552 and original valid: 727). The Chexpert-labeler [2] was used to assign the appropriate labels to the IU-RR images in order to be consistent with the labels provided for CheXpert and CheXphoto.

Multiple alternative labels for a target disease might create conflicting results between categories because our Zero-shot classification and case retrieval are focused on locating the most comparable target. Therefore, only five diseases were selected (atelectasis, cardiomegaly, edema, pleural effusion, and consolidation), and cases with only that disease were extracted from the database [1]. For CheXpert there are 87 positive images for each of the 5 diseases resulting in CheXphoto_5x87 dataset (total of 435 images). For CheXphoto there are 62 positive images for each of the five diseases resulting in the CheXphoto_5x62 dataset (total of 310 images). Each picture in this collection has a positive annotation for just one particular circumstance. Due to the fact that consolidation was only present in one instance, IU-RR 5x1 could only concentrate on one image per disease (5 cases in total).

The images from the above datasets are split into training, validation, and test sets. For the validation, Chexpert-labeler chooses 5,000 photos randomly from the original expert-labeled training sets for CheXpert and CheXphoto, respectively. For IU-RR Chexpert-labeler chose 500 photos at random from the original training

Table 1: Three datasets and their corresponding train, validation, and test splits, number of images, and details of each split are listed here.

Dataset split	Description	Number of images
CheXpert _{tr}	Frontal train split	185,778
CheXpert _{val}	Frontal validation split	4,301
CheXpert _{ts}	Frontal test	202
CheXphoto _{tr}	Frontal train split	23,512
CheXphoto _{val}	Frontal validation split	4,319
CheXphoto _{ts}	Frontal test	606
IU-RR _{tr}	Frontal train split	2,552
IU-RR _{ts}	Frontal test	727

Table 2: Evaluation of our representation learning performance based on supervised learning classification is listed here. The CheXphoto dataset [88] is used as a noisy dataset to train a classifier based on our representation learning. Both the representation learning dataset and test dataset are from IU-RR [2].

Train	Valid	Test	Train AUC	Valid AUC	Test AUC
CheXpert _{tr}	CheXpert _{val}	IU-RR _{ts}	0.680	0.681	0.856
CheXpert _{tr}	CheXphoto _{val}	IU-RR _{ts}	0.676	0.644	0.865
CheXpert _{tr}	IU-RR _{tr}	IU-RR _{ts}	0.674	0.881	0.868
CheXphoto _{tr}	CheXphoto _{val}	IU-RR _{ts}	0.643	0.619	0.862
CheXphoto _{tr}	CheXpert _{val}	IU-RR _{ts}	0.614	0.643	0.860
CheXphoto _{tr}	IU-RR _{tr}	IU-RR _{ts}	0.636	0.868	0.860

set because of the smaller IU-RR dataset. The training sets for all three datasets are determined by what is left after the corresponding validation sets are selected. Then, from the expert-labeled training file, CheXpert 5x87, CheXphoto 5x62, and IU-RR 5x1 are generated with exclusively positive images. Lastly, the untouched expert-labeled validation file is used as an independent test. Therefore, for CheXpert the frontal train split (CheXpert_{tr}) consists of 185,778 images, the frontal validation split (CheXpert_{val}) is 4,301 images, and the frontal test (CheXpert_{ts}) is 202 images. For CheXphoto the frontal train split (CheXphoto_{tr}) is 23,512 images, the frontal validation split (CheXphoto_{val}) is 4,319 images, and the frontal test (CheXphoto_{ts}) is 606 images. For IU-RR, the frontal train split (IU-RR_{tr}) is 2,552 images, and the frontal test (IU-RR_{ts}) is 727 images. The number of images in each split of these datasets is listed in Table 1.

4. EXPERIMENTS

We use the codes from the <https://github.com/marshuang80/gloria>, and use their zero-shot classification and supervised classification to evaluate the performance of our representation learning based on the IU-RR dataset that we cleaned and prepared. Area Under the Curve (AUC) is used as the performance metric for these downstream tasks.

Supervised classification The goal here is to evaluate the performance of the representation learning on IU-RR dataset based on the performance of the supervised learning problem. To this end, we train the model based on the small-size, publicly available dataset of IU-RR [2]. Consequently, we use noisy data of CheXphoto to

Table 3: Zero-shot classification performance based on the representation model trained on IU-RR dataset

	Atelectasis	Cardiomegaly	Consolidation	Edema	Pleural Effusion	Average
CheXpert	0.685	0.628	0.694	0.754	0.717	0.696
CheXphoto	0.719	0.587	0.700	0.784	0.694	0.697

train the classifier based on our encoder. The results are listed in Table 2. As listed in Table 2, the performance of the classifier achieves the AUC of 0.8618 ± 0.0042 (Mean + STD), which is slightly lower than the best of the previously reported values in [89], which is 0.8608. The reason that the test is higher than validation and the train is that the test is on a different data set.

Zero-shot classification: The model here has been applied to three different datasets in various configurations, noting that radiology reports of CheXpert and CheXphoto are not publicly available. Therefore we rely on the IU-RR dataset for the training of the representation learning. However, due to the smaller size of the IU-RR dataset compared to the two other datasets, the zero-shot learning is the model trained on the CheXpert dataset [1]. We compare the performance of the zero-shot classification based on representations that are learned on IU-RR, CheXpert, and CheXphoto, and based on five types of lung diseases, namely atelectasis, cardiomegaly, edema, pleural, and effusion. The detailed values of the classification results are listed in Table 3.

For comparison, the average AUC for classifying the five lung pathologies on the IU-RR test set ranged from 0.85 to 0.87 using the different training datasets. These results compare favorably to other studies using IU-RR for the classification of the five lung pathologies (AUC range:0.77-0.86) reported in the literature [89].

5. CONCLUSION

We developed a model that uses independent datasets utilizing language and vision modalities to learn a representation encompassing local and global features. The clinical significance of the model is the ability to utilize both image features from the X-Rays and text characteristics from reports to classify lung pathologies on chest X-rays. Five lung pathologies (atelectasis, cardiomegaly, edema, pleural, and consolidation) were considered. The average AUC for classifying the five lung pathologies on the IU-RR test set ranged from 0.85 to 0.87 using the different training datasets. These results compare favorably to other studies using UI-RR to classify the five lung pathologies with a mean AUC of 0.86, which is favorably comparable to existing literature. We have validated the cross-modal model on three independent datasets: IU-RR, CheXpert, and CheXphoto. The robust performance of the model on different datasets is promising and shows that it behaves satisfactorily.

ACKNOWLEDGMENTS

This research was partially funded by the American College of Radiology (ACR) Innovation Award “AI-PROBE: A Novel Prospective Randomized Clinical Trial Approach for Investigating the Clinical Usefulness of Artificial Intelligence in Radiology” (PI: Axel Wismüller) and an Ernest J. Del Monte Institute for Neuroscience Award from the Harry T. Mangurian Jr. Foundation (PI: Axel Wismüller). This work was conducted as a Practice Quality Improvement (PQI) project related to the American Board of Radiology (ABR) Maintenance of Certificate (MOC) for A.W.

REFERENCES

- [1] Huang, S.-C., Shen, L., Lungren, M. P., and Yeung, S., "Gloria: A multimodal global-local representation learning framework for label-efficient medical image recognition," in *[Proceedings of the IEEE/CVF International Conference on Computer Vision]*, 3942–3951 (2021).
- [2] Demner-Fushman, D., Kohli, M. D., Rosenman, M. B., Shooshan, S. E., Rodriguez, L., Antani, S., Thoma, G. R., and McDonald, C. J., "Preparing a collection of radiology examinations for distribution and retrieval," *Journal of the American Medical Informatics Association* **23**(2), 304–310 (2016).
- [3] Bunte, K., Hammer, B., Wismüller, A., and Biehl, M., "Adaptive local dissimilarity measures for discriminative dimension reduction of labeled data," *Neurocomputing* **73**(7-9), 1074–1092 (2010).
- [4] Wismüller, A., Vietze, F., and Dersch, D. R., "Segmentation with neural networks," in *[Handbook of medical imaging]*, 107–126, Academic Press, Inc. (2000).
- [5] Wismüller, A., Vietze, F., Behrends, J., Meyer-Baese, A., Reiser, M., and Ritter, H., "Fully automated biomedical image segmentation by self-organized model adaptation," *Neural Networks* **17**(8-9), 1327–1344 (2004).
- [6] Hoole, P., Wismüller, A., Leinsinger, G., Kroos, C., Geumann, A., and Inoue, M., "Analysis of tongue configuration in multi-speaker, multi-volume MRI data," (2000).
- [7] Wismüller, A., "Exploratory morphogenesis (XOM): a novel computational framework for self-organization," *Ph. D. thesis, Technical University of Munich, Department of Electrical and Computer Engineering* (2006).
- [8] Wismüller, A., Dersch, D. R., Lipinski, B., Hahn, K., and Auer, D., "A neural network approach to functional MRI pattern analysis—clustering of time-series by hierarchical vector quantization," in *[International Conference on Artificial Neural Networks]*, 857–862, Springer (1998).
- [9] Wismüller, A., Vietze, F., Dersch, D. R., Behrends, J., Hahn, K., and Ritter, H., "The deformable feature map—a novel neurocomputing algorithm for adaptive plasticity in pattern analysis," *Neurocomputing* **48**(1-4), 107–139 (2002).
- [10] Behrends, J., Hoole, P., Leinsinger, G. L., Tillmann, H. G., Hahn, K., Reiser, M., and Wismüller, A., "A segmentation and analysis method for MRI data of the human vocal tract," in *[Bildverarbeitung für die Medizin 2003]*, 186–190, Springer (2003).
- [11] Wismüller, A., "Neural network computation in biomedical research: chances for conceptual cross-fertilization," *Theory in Biosciences* (1997).
- [12] Bunte, K., Hammer, B., Villmann, T., Biehl, M., and Wismüller, A., "Exploratory observation machine (XOM) with Kullback-Leibler divergence for dimensionality reduction and visualization," in *[ESANN]*, **10**, 87–92 (2010).
- [13] Wismüller, A., Vietze, F., Dersch, D. R., Hahn, K., and Ritter, H., "The deformable feature map—adaptive plasticity for function approximation," in *[International Conference on Artificial Neural Networks]*, 123–128, Springer (1998).
- [14] Wismüller, A., "The exploration machine—a novel method for data visualization," in *[International Workshop on Self-Organizing Maps]*, 344–352, Springer (2009).
- [15] Huber, M. B., Nagarajan, M., Leinsinger, G., Ray, L. A., and Wismüller, A., "Classification of interstitial lung disease patterns with topological texture features," in *[Medical Imaging 2010: Computer-Aided Diagnosis]*, **7624**, 762410, International Society for Optics and Photonics (2010).
- [16] Wismüller, A., "The exploration machine: a novel method for analyzing high-dimensional data in computer-aided diagnosis," in *[Medical Imaging 2009: Computer-Aided Diagnosis]*, **7260**, 72600G, International Society for Optics and Photonics (2009).
- [17] Bunte, K., Hammer, B., Villmann, T., Biehl, M., and Wismüller, A., "Neighbor embedding XOM for dimension reduction and visualization," *Neurocomputing* **74**(9), 1340–1350 (2011).
- [18] Meyer-Bäse, A., Lange, O., Wismüller, A., and Ritter, H., "Model-free functional MRI analysis using topographic independent component analysis," *International journal of neural systems* **14**(04), 217–228 (2004).
- [19] Wismüller, A., "Exploration-organized morphogenesis (XOM): A general framework for learning by self-organization," *Forschungsberichte-Institut für Phonetik und Sprachliche Kommunikation der Universität München* (37), 205–239 (2001).
- [20] Saalbach, A., Twellmann, T., Nattkemper, T. W., Wismüller, A., Ontrup, J., and Ritter, H. J., "A hyperbolic topographic mapping for proximity data," in *[Artificial Intelligence and Applications]*, **2005**, 106–111 (2005).
- [21] Wismüller, A., "A computational framework for nonlinear dimensionality reduction and clustering," in *[International Workshop on Self-Organizing Maps]*, 334–343, Springer (2009).
- [22] Leinsinger, G., Teipel, S., Wismüller, A., Born, C., Meindl, T., Flatz, W., Schönberg, S., Pruessner, J., Hampel, H., and Reiser, M., "Volumetric MRI for evaluation of regional pattern and progression of neocortical degeneration in alzheimer's disease," *Der Radiologe* **43**(7), 537–542 (2003).
- [23] Meyer-Bäse, A., Auer, D., and Wismüller, A., "Topographic independent component analysis for fMRI signal detection," in *[Proceedings of the International Joint Conference on Neural Networks, 2003.]*, **1**, 601–605, IEEE (2003).
- [24] Wismüller, A., "The exploration machine—a novel method for structure-preserving dimensionality reduction," in *[ESANN]*, Citeseer (2009).
- [25] Wismüller, A., Lange, O., Auer, D., and Leinsinger, G., "Model-free functional MRI analysis for detecting low-frequency functional connectivity in the human brain," in *[Medical Imaging 2010: Computer-Aided Diagnosis]*, **7624**, 76241M, International Society for Optics and Photonics (2010).
- [26] Meyer-Bäse, A., Schlossbauer, T., Lange, O., and Wismüller, A., "Small lesions evaluation based on unsupervised cluster analysis of signal-intensity time courses in dynamic breast MRI," *International journal of biomedical imaging* **2009** (2009).
- [27] Meyer-Bäse, A., Saalbach, A., Lange, O., and Wismüller, A., "Unsupervised clustering of fMRI and MRI time series," *Biomedical Signal Processing and Control* **2**(4), 295–310 (2007).
- [28] Wismüller, A., Verleysen, M., Aupetit, M., and Lee, J. A., "Recent advances in nonlinear dimensionality reduction, manifold and topological learning," in *[ESANN]*, (2010).
- [29] Meyer-Bäse, A., Lange, O., Wismüller, A., and Hurdal, M. K., "Analysis of dynamic susceptibility contrast MRI time series based on unsupervised clustering methods," *IEEE Transactions on Information Technology in Biomedicine* **11**(5), 563–573 (2007).
- [30] Wismüller, A., Vietze, F., Dersch, D. R., Hahn, K., and Ritter, H. J., "A neural network approach to adaptive pattern analysis—the deformable feature map," in *[ESANN]*, 189–194 (2000).
- [31] Wismüller, A., Behrends, J., Hoole, P., Leinsinger, G. L., Reiser, M. F., and Westesson, P.-L., "Human vocal tract analysis by in vivo 3d MRI during phonation: a complete system for imaging, quantitative modeling, and speech synthesis," in *[International Conference on Medical Image Computing and Computer-Assisted Intervention]*, 306–312, Springer (2008).
- [32] Wismüller, A., Dersch, D. R., Lipinski, B., Hahn, K., and Auer, D., "Hierarchical clustering of functional MRI time-series by deterministic annealing," in *[International Symposium on Medical Data Analysis]*, 49–54, Springer (2000).
- [33] Wismüller, A., "Method and device for representing multichannel image data," (Nov. 17 2015). US Patent 9,189,846.
- [34] Huber, M. B., Bunte, K., Nagarajan, M. B., Biehl, M., Ray, L. A., and Wismüller, A., "Texture feature ranking with relevance learning to classify interstitial lung disease patterns," *Artificial intelligence in medicine* **56**(2), 91–97 (2012).
- [35] Wismüller, A., Meyer-Bäse, A., Lange, O., Reiser, M. F., and Leinsinger, G., "Cluster analysis of dynamic cerebral contrast-enhanced perfusion MRI time-series," *IEEE transactions on medical imaging* **25**(1), 62–73 (2005).
- [36] Twellmann, T., Saalbach, A., Muller, C., Nattkemper, T. W., and Wismüller, A., "Detection of suspicious lesions in dynamic contrast enhanced MRI data," in *[The 26th Annual International Conference of the IEEE Engineering in Medicine and Biology Society]*, **1**, 454–457, IEEE (2004).
- [37] Otto, T. D., Meyer-Bäse, A., Hurdal, M., Summers, D., Auer, D., and Wismüller, A., "Model-free functional MRI analysis using cluster-based methods," in *[Intelligent Computing: Theory and Applications]*, **5103**, 17–24, International Society for Optics and Photonics (2003).
- [38] Varini, C., Nattkemper, T. W., Degenhard, A., and Wismüller, A., "Breast MRI data analysis by IIC," in *[2004 IEEE International Joint Conference on Neural Networks (IEEE Cat. No. 04CH37541)]*, **3**, 2449–2454, IEEE (2004).
- [39] Meyer-Bäse, A., Lange, O., Wismüller, A., and Leinsinger, G., "Computer-aided diagnosis in breast MRI based on ICA and unsupervised clustering techniques," in *[Independent Component Analyses, Wavelets, Unsupervised Smart Sensors, and Neural Networks III]*, **5818**, 38–49, International Society for Optics and Photonics (2005).
- [40] Huber, M. B., Lancianese, S. L., Nagarajan, M. B., Ikpot, I. Z., Lerner, A. L., and Wismüller, A., "Prediction of biomechanical properties of trabecular bone in mr images with geometric features and support vector regression," *IEEE Transactions on Biomedical Engineering* **58**(6), 1820–1826 (2011).
- [41] Meyer-Bäse, A., Pilyugin, S. S., and Wismüller, A., "Stability analysis of a self-organizing neural network with feedforward and feedback dynamics," in *[2004 IEEE International Joint Conference on Neural Networks (IEEE Cat. No. 04CH37541)]*, **2**, 1505–1509, IEEE (2004).
- [42] Wismüller, A., Dersch, D., Lipinski, B., Hahn, K., and Auer, D., "Hierarchical clustering of fMRI time-series by deterministic annealing," *Neuroimage* **7**(4), S593 (1998).
- [43] Meyer-Bäse, A., Lange, O., Schlossbauer, T., and Wismüller, A., "Computer-aided diagnosis and visualization based on clustering and independent component analysis for breast MRI," in *[2008 15th IEEE International Conference on Image Processing]*, 3000–3003, IEEE (2008).
- [44] Wismüller, A., De, T., Lochmüller, E., Eckstein, F., and Nagarajan, M. B., "Introducing anisotropic minkowski functionals and quantitative anisotropy measures for local structure analysis in biomedical imaging," in *[Medical Imaging 2013: Biomedical Applications in Molecular, Structural, and Functional Imaging]*, **8672**, 86720I, International Society for Optics and Photonics (2013).

- [45] Bhole, C., Pal, C., Rim, D., and Wismüller, A., "3d segmentation of abdominal ct imagery with graphical models, conditional random fields and learning," *Machine vision and applications* **25**(2), 301–325 (2014).
- [46] Nagarajan, M. B., Coan, P., Huber, M. B., Diemoz, P. C., Glaser, C., and Wismüller, A., "Computer-aided diagnosis in phase contrast imaging x-ray computed tomography for quantitative characterization of ex vivo human patellar cartilage," *IEEE Transactions on Biomedical Engineering* **60**(10), 2896–2903 (2013).
- [47] Wismüller, A., Behrends, J., Dersch, D., Leinsinger, G., Vietze, F., and Hahn, K., "Automatic segmentation of cerebral contours in multispectral MRI data sets of the human brain by self-organizing neural networks," in *[Radiology]*, **221**, 461–461 (2001).
- [48] Wismüller, A., Vietze, F., Dersch, D., Leinsinger, G., Ritter, H., and Hahn, K., "Adaptive self-organized template matching of the gray-level feature space for automatic segmentation of multispectral MRI data of the human brain," in *[Radiology]*, **213**, 364–364 (1999).
- [49] Meyer-Baese, A., Wismüller, A., Lange, O., and Leinsinger, G., "Computer-aided diagnosis in breast MRI based on unsupervised clustering techniques," in *[Intelligent Computing: Theory and Applications II]*, **5421**, 29–37, International Society for Optics and Photonics (2004).
- [50] Nagarajan, M. B., Coan, P., Huber, M. B., Diemoz, P. C., Glaser, C., and Wismüller, A., "Computer-aided diagnosis for phase-contrast x-ray computed tomography: quantitative characterization of human patellar cartilage with high-dimensional geometric features," *Journal of digital imaging* **27**(1), 98–107 (2014).
- [51] Pester, B., Leistritz, L., Witte, H., and Wismüller, A., "Exploring effective connectivity by a Granger causality approach with embedded dimension reduction," *Biomedical Engineering/Biomedizinische Technik* **58**(SI-1-Track-G), 00001015120134172 (2013).
- [52] Nagarajan, M. B., Huber, M. B., Schlossbauer, T., Leinsinger, G., Krol, A., and Wismüller, A., "Classification of small lesions on dynamic breast MRI: Integrating dimension reduction and out-of-sample extension into cadx methodology," *Artificial intelligence in medicine* **60**(1), 65–77 (2014).
- [53] Yang, C.-C., Nagarajan, M. B., Huber, M. B., Carballido-Gamio, J., Bauer, J. S., Baum, T. H., Eckstein, F., Lochmüller, E.-M., Majumdar, S., Link, T. M., et al., "Improving bone strength prediction in human proximal femur specimens through geometrical characterization of trabecular bone microarchitecture and support vector regression," *Journal of electronic imaging* **23**(1), 013013 (2014).
- [54] Wismüller, A., Nagarajan, M. B., Witte, H., Pester, B., and Leistritz, L., "Pair-wise clustering of large scale Granger causality index matrices for revealing communities," in *[Medical Imaging 2014: Biomedical Applications in Molecular, Structural, and Functional Imaging]*, **9038**, 90381R, International Society for Optics and Photonics (2014).
- [55] Wang, X., Nagarajan, M. B., Conover, D., Ning, R., O'Connell, A., and Wismüller, A., "Investigating the use of texture features for analysis of breast lesions on contrast-enhanced cone beam CT," in *[Medical Imaging 2014: Biomedical Applications in Molecular, Structural, and Functional Imaging]*, **9038**, 903822, International Society for Optics and Photonics (2014).
- [56] Wismüller, A., Wang, X., DSouza, A. M., and Nagarajan, M. B., "A framework for exploring non-linear functional connectivity and causality in the human brain: mutual connectivity analysis (mca) of resting-state functional MRI with convergent cross-mapping and non-metric clustering," *arXiv preprint arXiv:1407.3809* (2014).
- [57] Meyer-Bäse, A., Pilyugin, S., Wismüller, A., and Foo, S., "Local exponential stability of competitive neural networks with different time scales," *Engineering Applications of Artificial Intelligence* **17**(3), 227–232 (2004).
- [58] Schmidt, C., Pester, B., Nagarajan, M., Witte, H., Leistritz, L., and Wismüller, A., "Impact of multivariate Granger causality analyses with embedded dimension reduction on network modules," in *[2014 36th Annual International Conference of the IEEE Engineering in Medicine and Biology Society]*, 2797–2800, IEEE (2014).
- [59] Nagarajan, M. B., Coan, P., Huber, M. B., Diemoz, P. C., and Wismüller, A., "Integrating dimension reduction and out-of-sample extension in automated classification of ex vivo human patellar cartilage on phase contrast x-ray computed tomography," *Plos one* **10**(2), e0117157 (2015).
- [60] Wismüller, A., Abidin, A. Z., D'Souza, A. M., Wang, X., Hobbs, S. K., Leistritz, L., and Nagarajan, M. B., "Nonlinear functional connectivity network recovery in the human brain with mutual connectivity analysis (MCA): convergent cross-mapping and non-metric clustering," in *[Medical Imaging 2015: Biomedical Applications in Molecular, Structural, and Functional Imaging]*, **9417**, 94170M, International Society for Optics and Photonics (2015).
- [61] Nagarajan, M. B., Chechefsky, W. A., Abidin, A. Z., Tsai, H., Wang, X., Hobbs, S. K., Bauer, J. S., Baum, T., and Wismüller, A., "Characterizing trabecular bone structure for assessing vertebral fracture risk on volumetric quantitative computed tomography," in *[Medical Imaging 2015: Biomedical Applications in Molecular, Structural, and Functional Imaging]*, **9417**, 94171E, International Society for Optics and Photonics (2015).
- [62] Abidin, A. Z., Nagarajan, M. B., Chechefsky, W. A., Coan, P., Diemoz, P. C., Hobbs, S. K., Huber, M. B., and Wismüller, A., "Volumetric characterization of human patellar cartilage matrix on phase contrast x-ray computed tomography," in *[Medical Imaging 2015: Biomedical Applications in Molecular, Structural, and Functional Imaging]*, **9417**, 94171F, International Society for Optics and Photonics (2015).
- [63] Wismüller, A., Abidin, A. Z., DSouza, A. M., and Nagarajan, M. B., "Mutual connectivity analysis (MCA) for nonlinear functional connectivity network recovery in the human brain using convergent cross-mapping and non-metric clustering," in *[Advances in Self-Organizing Maps and Learning Vector Quantization]*, 217–226, Springer (2016).
- [64] Abidin, A. Z., D'Souza, A. M., Nagarajan, M. B., and Wismüller, A., "Investigating changes in brain network properties in hiv-associated neurocognitive disease (HAND) using mutual connectivity analysis (MCA)," in *[Medical Imaging 2016: Biomedical Applications in Molecular, Structural, and Functional Imaging]*, **9788**, 97881W, International Society for Optics and Photonics (2016).
- [65] Schmidt, C., Pester, B., Schmid-Hertel, N., Witte, H., Wismüller, A., and Leistritz, L., "A multivariate Granger causality concept towards full brain functional connectivity," *PloS one* **11**(4) (2016).
- [66] Abidin, A. Z., Jameson, J., Molthen, R., and Wismüller, A., "Classification of micro-CT images using 3D characterization of bone canal patterns in human osteogenesis imperfecta," in *[Medical-Aided Diagnosis]*, **10134**, 1013413, International Society for Optics and Photonics (2017).
- [67] Abidin, A. Z., Chockanathan, U., DSouza, A. M., Inglese, M., and Wismüller, A., "Using large-scale Granger causality to study changes in brain network properties in the clinically isolated syndrome (CIS) stage of multiple sclerosis," in *[Medical Imaging 2017: Biomedical Applications in Molecular, Structural, and Functional Imaging]*, **10137**, 101371B, International Society for Optics and Photonics (2017).
- [68] DSouza, A. M., Abidin, A. Z., Leistritz, L., and Wismüller, A., "Exploring connectivity with large-scale Granger causality on resting-state functional MRI," *Journal of neuroscience methods* **287**, 68–79 (2017).
- [69] Abidin, A. Z., DSouza, A. M., Nagarajan, M. B., Wang, L., Qiu, X., Schifitto, G., and Wismüller, A., "Alteration of brain network topology in HIV-associated neurocognitive disorder: A novel functional connectivity perspective," *NeuroImage: Clinical* **17**, 768–777 (2018).
- [70] Abidin, A. Z., Deng, B., DSouza, A. M., Nagarajan, M. B., Coan, P., and Wismüller, A., "Deep transfer learning for characterizing chondrocyte patterns in phase contrast x-ray computed tomography images of the human patellar cartilage," *Computers in biology and medicine* **95**, 24–33 (2018).
- [71] Chockanathan, U., Abidin, A. Z., DSouza, A. M., Schifitto, G., and Wismüller, A., "Resilient modular small-world directed brain networks in healthy subjects with large-scale Granger causality analysis of resting-state functional MRI," in *[Medical Imaging 2018: Biomedical Applications in Molecular, Structural, and Functional Imaging]*, **10578**, 105780B, International Society for Optics and Photonics (2018).
- [72] DSouza, A. M., Abidin, A. Z., Chockanathan, U., Schifitto, G., and Wismüller, A., "Mutual connectivity analysis of resting-state functional MRI data with local models," *NeuroImage* **178**, 210–223 (2018).
- [73] Chockanathan, U., DSouza, A. M., Abidin, A. Z., Schifitto, G., and Wismüller, A., "Automated diagnosis of HIV-associated neurocognitive disorders using large-scale Granger causality analysis of resting-state functional MRI," *Computers in Biology and Medicine* **106**, 24–30 (2019).
- [74] Abidin, A. Z., Dar, I., D'Souza, A. M., Lin, E. P., and Wismüller, A., "Investigating a quantitative radiomics approach for brain tumor classification," in *[Medical Imaging 2019: Biomedical Applications in Molecular, Structural, and Functional Imaging]*, **10953**, 109530B, International Society for Optics and Photonics (2019).
- [75] DSouza, A. M., Abidin, A. Z., and Wismüller, A., "Classification of autism spectrum disorder from resting-state fMRI with mutual connectivity analysis," in *[Medical Imaging 2019: Biomedical Applications in Molecular, Structural, and Functional Imaging]*, **10953**, 109531D, International Society for Optics and Photonics (2019).
- [76] Abidin, A. Z., DSouza, A. M., Schifitto, G., and Wismüller, A., "Detecting cognitive impairment in HIV-infected individuals using mutual connectivity analysis of resting state functional MRI," *Journal of neurovirology* **26**(2), 188–200 (2020).
- [77] Wismüller, A. and Stockmaster, L., "A prospective randomized clinical trial for measuring radiology study reporting time on artificial intelligence-based detection of intracranial hemorrhage in emergent care head ct," in *[Medical Imaging 2020: Biomedical Applications in Molecular, Structural, and Functional Imaging]*, **11317**, 113170M, International Society for Optics and Photonics (2020).
- [78] Wismüller, A., DSouza, A. M., Abidin, A. Z., and Vosoughi, M. A., "Large-scale nonlinear Granger causality: A data-driven, multivariate approach to recovering directed networks from short time-series data," *arXiv preprint arXiv:2009.04681* (2020).
- [79] Vosoughi, A., DSouza, A., Abidin, A., and Wismüller, A., "Relation discovery in nonlinearly related large-scale settings," in *[ICASSP 2022-2022 IEEE International Conference on Acoustics, Speech and Signal Processing (ICASSP)]*, 5103–5107, IEEE (2022).
- [80] Vosoughi, M. A. and Wismüller, A., "Large-scale kernelized Granger causality to infer topology of directed graphs with applications to brain networks," *arXiv preprint arXiv:2011.08261* (2020).
- [81] Vosoughi, M. A. and Wismüller, A., "Large-scale extended granger causality for classification of marijuana users from functional mri," in *[Medical Imaging 2021: Biomedical Applications in Molecular, Structural, and Functional Imaging]*, **11600**, 116000D, International Society for Optics and Photonics (2021).

- [82] Wismüller, A. and Vosoughi, M. A., "Classification of schizophrenia from functional MRI using large-scale extended Granger causality," *International Society for Optics and Photonics* (2021).
- [83] Wismüller, A. and Vosoughi, M. A., "Large-scale augmented Granger causality (lsAGC) for connectivity analysis in complex systems: From computer simulations to functional MRI (fMRI)," in [*Medical Imaging 2021: Biomedical Applications in Molecular, Structural, and Functional Imaging*], **11600**, 1160009, International Society for Optics and Photonics (2021).
- [84] Wismüller, A., Dsouza, A. M., Vosoughi, M. A., and Abidin, A., "Large-scale nonlinear Granger causality for inferring directed dependence from short multivariate time-series data," *Scientific reports* **11**(1), 1–11 (2021).
- [85] Vosoughi, M. A. and Wismüller, A., "Leveraging pre-images to discover nonlinear relationships in multivariate environments," in [*2021 European Signal Processing Conference (EUSIPCO)*], IEEE (August 2021).
- [86] Vosoughi, M. A. and Wismüller, A., "Large-scale kernelized granger causality (lskge) for inferring topology of directed graphs in brain networks," in [*Medical Imaging 2022: Biomedical Applications in Molecular, Structural, and Functional Imaging*], **12036**, 1203603, SPIE (2022).
- [87] Irvin, J., Rajpurkar, P., Ko, M., Yu, Y., Ciurea-Ilcus, S., Chute, C., Marklund, H., Haghgoo, B., Ball, R., Shpanskaya, K., et al., "Chexpert: A large chest radiograph dataset with uncertainty labels and expert comparison," in [*Proceedings of the AAAI conference on artificial intelligence*], **33**(01), 590–597 (2019).
- [88] Phillips, N. A., Rajpurkar, P., Sabini, M., Krishnan, R., Zhou, S., Pareek, A., Phu, N. M., Wang, C., Jain, M., Du, N. D., et al., "Chexphoto: 10,000+ photos and transformations of chest x-rays for benchmarking deep learning robustness," in [*Machine Learning for Health*], 318–327, PMLR (2020).
- [89] Xue, Y. and Huang, X., "Improved disease classification in chest x-rays with transferred features from report generation," in [*International Conference on Information Processing in Medical Imaging*], 125–138, Springer (2019).